

Journal of Biomedical Optics

SPIEDigitalLibrary.org/jbo

Transcutaneous delivery of micro- and nanoparticles with laser microporation

Elina A. Genina
Alexey N. Bashkatov
Leonid E. Dolotov
Galina N. Maslyakova
Vyacheslav I. Kochubey
Ilya V. Yaroslavsky
Gregory B. Altshuler
Valery V. Tuchin

Transcutaneous delivery of micro- and nanoparticles with laser microporation

Elina A. Genina,^a Alexey N. Bashkatov,^a Leonid E. Dolotov,^a Galina N. Maslyakova,^b Vyacheslav I. Kochubey,^a Ilya V. Yaroslavsky,^c Gregory B. Altshuler,^c and Valery V. Tuchin^{a,d,e}

^aSaratov State University, Research-Educational Institute of Optics and Biophotonics, 83 Astrakhanskaya Street, Saratov 410012, Russia

^bSaratov State Medical University, Department of Pathological Anatomy, 112 Bolshaya Kazachia, Saratov 410012, Russia

^cCynosure Inc., 15 Network Drive, Burlington, Massachusetts 01803

^dInstitute of Precise Mechanics and Control of RAS, Laboratory of Laser Diagnostics of Technical and Living Systems, 24 Rabochaya Street, Saratov 410028, Russia

^eUniversity of Oulu, Optoelectronics and Measurement Techniques Laboratory, P.O. Box 4500, Oulu FIN-90014, Finland

Abstract. Fractional laser ablation is one of the relatively safe and minimally invasive methods used to administer micro- and nanoparticles into the skin at sufficiently large depth. In this article, we present the results of delivery of TiO₂ nanoparticles and Al₂O₃ microparticles into skin. Fractional laser microablation of skin was provided by a system based on a pulsed Er:YAG laser with the following parameters: the wavelength 2940 nm, the pulse energy 3.0 J, and the pulse duration 20 ms. *Ex vivo* and *in vivo* human skin was used in the study. The suspensions of titanium dioxide and alumina powder in polyethylene glycol with particle size of about 100 nm and 27 μ m, respectively, were used. In the *ex vivo* experiments, reflectance spectra of skin samples with administered particles were measured and histological sections of the samples were made. In the *in vivo* experiment, reflectance spectroscopy, optical coherence tomography, and clinical photography were used to monitor the skin status during one month after suspension administering. It is shown that particles can be delivered into dermis up to the depth 230 μ m and distributed uniformly in the tissue. Spectral measurements confirm that the particles stay in the dermis longer than 1 month. © 2013 Society of Photo-Optical Instrumentation Engineers (SPIE) [DOI: 10.1117/1.JBO.18.11.111406]

Keywords: fractional laser microablation; skin; TiO₂ nanoparticles; Al₂O₃ microparticles; optical coherence tomography; reflectance spectroscopy.

Paper 130124SSR received Mar. 6, 2013; revised manuscript received Jun. 13, 2013; accepted for publication Jun. 17, 2013; published online Jul. 15, 2013.

1 Introduction

There are many studies demonstrating the importance of transcutaneous drug delivery and ability to create a long-term reservoir in the dermis for topically applied compounds.^{1–3} The main advantages of transcutaneous administration of preparations are: (1) minimal invasiveness or even noninvasiveness; (2) improved drug pharmacokinetics; and (3) targeted drug delivery.¹ Many treatment protocols in dermatology, oncology, cosmetology, etc., are based on transcutaneous delivery.

However, the stratum corneum (SC) with the thickness in the range of 10 to 20 μ m and underlying living epidermis of thickness 75 to 150 μ m represents a barrier separating body from the environment and makes preparation delivery deep into the skin a rather difficult problem.^{1,4} Skin appendages play an important role as a penetration route at the topical application of drugs.^{1,5–8}

Recently, it was shown that nanoparticles are more suited to penetrate efficiently into the appendages, in particular, into hair follicles, than nonparticle substances.^{2,6} The penetration of micro- and nanoparticles into the skin can also occur through sebaceous gland ducts (diameter: 10 to 70 μ m),⁷ sweat gland ducts (diameter: 60 to 80 μ m),⁸ or aqueous pores, transpiercing the epidermis (diameter less than 10 nm).¹ Therefore, it is possible to use nanoparticles as drug carriers for efficient selective

drug delivery and storage of topically applied substances into skin appendages, which is important for selective dermatotherapy. However, density and dimensions of these naturally occurring pathways vary widely between anatomical sites and individuals. Besides, particles with a diameter of approximately 100 nm and more cannot pass out of the appendages into living tissue.⁹ Unlike nanoparticles, microparticles (> 10 μ m) penetrate neither into the follicular orifices nor into the SC, whereas the particles with the sizes 9 to 10 μ m concentrate around the openings of the follicles without further penetration.⁵ The smallest microspheres <3 μ m penetrate into the skin appendages well but are also observed in the superficial layers of SC and never in the viable epidermis.¹⁰ Therefore, for effective delivery of micro- and nanoparticles, strategies including complex physical enhancement methods have been developed, for example, magnetic field,¹¹ ultrasound treatment,¹² photomechanical waves,¹³ needleless injection,¹⁴ and artificial channels produced by the sonoporation,¹⁵ electroporation,¹⁶ mechanical,^{17,18} or laser action.¹⁹ Multimodal methods include combination of the microporation and ultrasound treatment.^{12,20} Recently, it was reported that also the application of cold tissue tolerable plasma was able to increase the penetration of topically applied nanoparticles.²¹

Creating artificial channels by means of microporation promotes deeper and more targeted delivery of particles. In this case, both the diameter and the depth of pores depend on

Address all correspondence to: Elina A. Genina, Saratov State University, Optics and Biophotonics Department, 83 Astrakhanskaya Street, Saratov 410012, Russia. Tel: +7 8452 270716; Fax: +7 8452 278529; E-mail: egenina@yandex.ru

0091-3286/2013/\$25.00 © 2013 SPIE

the instruments acting on the skin.¹ Thus, if the diameter of the thinnest standard needle, available at present, is 184 μm , the diameters of microneedles, used in the mechanical microporation, may reach $\sim 100 \mu\text{m}$, whereas the diameters of microchannels, created as a result of thermo- and electroporation, may be 10 to 50 μm .^{1,16} The mean depth of penetration of solid particles at needleless injection varies from $<10 \mu\text{m}$ to $>20 \mu\text{m}$.¹⁴ The micropore depth was determined to be about 250 μm when using the mechanical microporation approaches²² and when using laser fractional microablation, it can reach up to 1500 μm .²³

Fractional devices create thermally induced microchannels of damage in the skin. Depending on device parameters, the damage within these microchannels can be of nonablative (protein denaturation) and/or ablative (water vaporization) nature.²³ Fractional laser microablation (FLMA) is one of the relatively safe and minimally invasive methods used to administer micro- and nanoparticles into the skin at sufficiently large depth in comparison with surface ablation and mechanical treatments because of the low area of skin damage and, therefore, reduced risk of infection.^{1,23,24}

The variation in laser radiation parameters at FLMA provides a variable depth of microchannels^{20,23,25} and enables precise control of the depth of particle administering. Besides all advantages inherent in other microporation methods, FLMA allows for control not only of the depth but also of the cross-section of the microchannels by means of varying geometry of laser microbeams.^{20,23,25} The results of observations showed that the complete epidermal healing occurred within a week.^{24,25}

We used titanium dioxide (TiO_2) nanoparticles and alumina (Al_2O_3) microparticles as test compounds for the particle delivery experiments. It is known that metal nanoparticles have a great potential for enhancement of skin image contrast in optical imaging modalities, such as optical coherent tomography,²⁶ confocal laser scanning microscopy,²⁷ and multiphoton microscopy.²⁸ TiO_2 and Al_2O_3 particles can be effective contrast agents for optical coherence tomography (OCT) imaging due to high scattering properties and comparatively low absorption in the near infrared (NIR) range.^{26,29} Besides, TiO_2 nanoparticles are widely used in cosmetic production for protection against detrimental effects of UV radiation and personal care products.^{30,31} Al_2O_3 is inert cosmetic-grade material.³² It functions in cosmetics as an abrasive, absorbent, anticaking agent, bulking agent, and opacifying agent.³³

In this article, we are presenting results on delivery of TiO_2 nanoparticles and Al_2O_3 microparticles into skin using the FLMA of the skin surface with the view of developing a reliable and reproducible method of nano- and microparticle delivery in the tissue. Besides, we examined the assumption that scattering properties of the particles could allow increasing skin scattering for improving skin appearance and other medical and cosmetic applications.

2 Methods and Materials

2.1 Laser System

To overcome the protective skin barrier, the technique of laser microablation of the surface layers of skin was developed. The commercially available Palomar Lux2940 erbium laser (Palomar Medical Technologies Inc., Burlington, MA) was used as a light source. The laser parameters were as follows: the wavelength 2940 nm, the pulse energy 3.0 J, and the pulse

duration 20 ms. The temporal profile of the laser pulse was modulated with three subpulses, with the subpulses' duration of 5 ms. The laser emission beam was split into 169 microbeams using an array of microlenslets. Vertical microchannels (169) were created in the skin in the area with the dimensions of $6 \times 6 \text{ mm}$. The separation between the centers of the channels was $\sim 500 \mu\text{m}$, diameter of their openings at skin surface was $\sim 100 \mu\text{m}$, and the depth was $\sim 300 \mu\text{m}$.

2.2 Preparation of Particle Suspensions

We used the TiO_2 nanopowder (634662-100G, Sigma-Aldrich Co., St. Louis, Missouri) consisting of a mixture of rutile and anatase TiO_2 with the particle size $<100 \text{ nm}$ and Al_2O_3 microparticles (LOMO PLC, Russia) with the particle size $\sim 27 \mu\text{m}$.

Absorption spectra of the particles (the fraction of light absorbed by the particles) were measured with a commercially available spectrophotometer Lambda 950 (PerkinElmer Inc., Waltham, Massachusetts) with an integrating sphere in the spectral range 320 to 1000 nm. Measurement of sample absorption is possible using the center-mount option of the spectrophotometer, in which the sample is suspended in the middle of the integrating sphere.³⁴ The studied powders were put into a quartz cuvette with the dimensions $20 \times 40 \text{ mm}$ and the thickness 2 mm. The cuvette was suspended in the middle of the sphere at the angle of 15 deg in relation to incident beam to exclude the specular reflection.

To enhance the penetration depth of the particles into the skin and to suppress the photocatalytic action of photochemically active anatase form of TiO_2 , the particles were suspended in polyethylene glycol (PEG-300) having the molecular weight 300 (Sigma-Aldrich Co.). The pH of the chemical measured with a test-paper (Erba Lachema s.r.o., Czechia) was 6. The refractive index of the PEG-300 was measured with an Abbe refractometer (Atago DR-M2/1550, Japan) at several wavelengths (450, 589, 680, 1100, and 1550 nm) and interpolated. It was evaluated as 1.457 at 930 nm. Refractive indices of TiO_2 and Al_2O_3 in the studied spectral range were 2.3 and 1.69, respectively.³⁵ The concentration of both nanoparticles and microparticles in the suspensions was 0.5 mg/mL. This concentration does not exceed the concentration of TiO_2 and Al_2O_3 permitted in cosmetics. The content of TiO_2 in personal care products and sunscreens is from 1% to $>10\%$ by weight.³⁰ Al_2O_3 microparticles were reported to be used in cosmetic products at concentrations up to 60%; and in skin care preparations, its concentration could be up to 25%.³³

The suspension was prepared using the CT-400A ultrasonic bath (CTBrand, Wan Luen Electronic Tools Co. Ltd., China) with the power of 35 W and the frequency of 43 to 45 kHz. The cuvette with the suspension was placed into the ultrasonic bath for 30 min for thorough mixing of the content both in the process of preparation and immediately before use.

2.3 Nanoparticle Delivery

The *ex vivo* experiments were carried out with four samples of human skin extracted in the course of autopsy. The dimensions of the samples were approximately $60 \times 20 \text{ mm}$, and the average thickness was $3.5 \pm 0.2 \text{ mm}$. Each sample was divided into three sites. Both the first and the second sites were microporated. The third one remained intact. After microchannels were created, the TiO_2 nanoparticle and Al_2O_3 microparticle suspensions were applied on the surface of the first site and the

second site, respectively. The total exposure time was 2 h. During the procedure, the samples were placed in a Petri dish with a small volume of saline (aqueous solution of NaCl with the concentration 0.9 mg/mL) to prevent the change in the optical properties due to dehydration. Then, the suspensions were removed from the skin surface with a tampon wetted with saline. The remains of the suspensions were removed using the Multifilm medical sticky tape (Tesa, Germany) by two surface strips. The mean thickness of each strip of epidermis was about 0.5 μm .³⁶ The reflectance spectra from each site of the studied samples were measured. All experiments were carried out at room temperature ($\sim 20^\circ\text{C}$).

The *in vivo* study was carried out with three volunteers. The treated area was chosen on a forearm and was divided into three sites. Before commencing the experiment, the skin was disinfected with 70% ethanol. Both the first and the second sites were microporated. The third one remained intact. The TiO_2 nanoparticle and Al_2O_3 microparticle suspensions were applied on the surface of the first site and the second site, respectively. The third one was also topically treated with TiO_2 suspension. The solution of chlorhexidine was added to the suspension in the proportion 2:3 to prevent the infection of the target skin areas. After the fractional microablation, the particle application, and hand massage for 5 min, the treated sites were covered by polyethylene film and bandaged for 2 h. Then, the particles were removed from the skin surface by distilled water.

The observations were carried out over a month period: intact skin before the treatment, immediately after the FLMA, in 2 h, 24 h, 6 days, 14 days, and 30 days after the treatment.

Each observation included skin surface photography using the Nikon D80 camera (Nikon Inc., Japan) equipped with the Micro-Nikkor macro objective (Nikon Inc.), the measurements of the reflectance spectra from the studied areas of skin, and OCT scanning.

2.4 Reflectance Measurements

The reflectance spectra of skin were measured using the USB4000-Vis-NIR multichannel spectrometer (Ocean Optics Inc., Dunedin, Florida) in the spectral range 380 to 1000 nm. The HL-2000 halogen lamp (Ocean Optics Inc., Dunedin, Florida) served as a source of light. The QR400-7-Vis/NIR fiber-optic probe (Ocean Optics Inc., Dunedin, Florida) consisting of seven fibers with the internal diameter 400 μm and the numerical aperture 0.2 was used in the measurements. The central fiber served for collecting the diffuse reflected radiation, while the surrounding six fibers were used for the illumination of the sample. The probe was placed at the distance of 2 mm from the skin surface and registered the signal averaged over the area of the radiation collection. The WS-1-SL reflectance standard (Ocean Optics Inc., Dunedin, Florida) was used to normalize the reflectance spectra.

2.5 Optical Coherence Tomography

Visualization of microchannels filled with the suspension of the particles was implemented using a commercial OCT system (model OCP930SR, Thorlabs, USA)³⁷ working at the central wavelength 930 ± 5 nm with 100 ± 5 nm full width at half maximum (FWHM) spectrum, an optical power of 2 mW, a maximum image depth of 1.6 mm, and a length of scanned area 6 mm. The axial resolution (A-FWHM) determined by the spectral bandwidth of the light source was 6.2 μm in air.

The lateral resolution (L-FWHM), entirely determined by the spatial focusing power of the objective, was 9.6 μm . In the medium, the parameters A-FWHM and L-FWHM increased.³⁸ If we suppose that the average refractive index of skin is about 1.42,³⁹ the axial and lateral resolutions can be evaluated as ~ 4.5 and ~ 7 μm , respectively.

The optical probing depth of skin was evaluated from OCT A-scan as a level where intensity of OCT signal decreased by a factor of e .

2.6 Histology Microscopic Study

Using the standard technique, the histological sections were prepared from the skin samples *ex vivo*. After fixation of the material with 10% solution of formalin, the samples were transferred through baths of progressively more concentrated ethanol to remove the water and then embedded in paraffin. The paraffin sections of 6 to 8 μm thickness were stained with haematoxylin and eosin.

The histological description of the preparations was carried out using the MC 100 XP microscope (Micros, Austria) operating in transmitted light mode with the magnification 200 \times . Photographs were taken using the Canon PC 1107 camera (Canon Inc., Japan).

3 Results

3.1 Histology Microscopic Study

Figure 1 presents microscopic images of histological sections of the skin sample *ex vivo* after FLMA with administering the TiO_2 nanoparticle suspension into the skin. In the images in light background, the nanoparticle suspension appears as a dark inclusion (marked with arrows). Figure 1(a) shows an individual microchannel produced by FLMA. In this case, the suspension is observed as a thin layer along the walls of the channel. The depth of penetration of nanoparticles coincides with that of the channel. Figure 1(b) shows the area between the channels. As it can be seen, the unassisted topical application of the suspension has resulted in very superficial penetration of the compound, not extending beyond the boundaries of epidermis. The compound has mostly stayed on skin surface and filled the hollows in

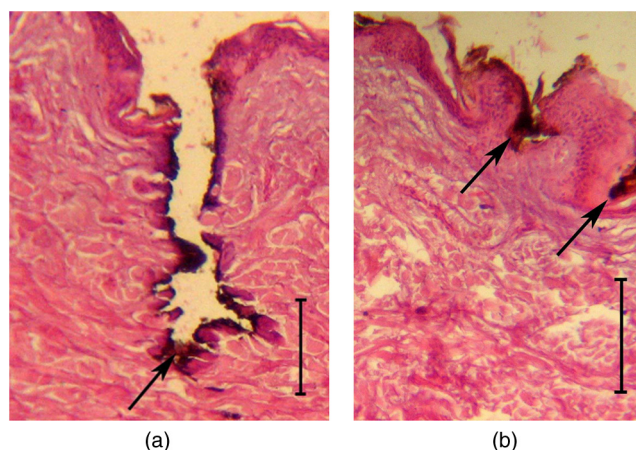


Fig. 1 Microscopic images of histological sections of the human skin samples *ex vivo* after the fractional laser microablation (FLMA) with administering the suspension into the skin (a) and unassisted topical application of TiO_2 nanoparticle suspension (b). Bars correspond to 100 μm . Arrows indicate the nanoparticles localization.

epidermal layer including openings of cutaneous sweat glands and follicles to the depth of less than 100 μm [Fig. 1(b)].

3.2 Ex vivo Experiments

Spectra of the light fraction absorbed in the studied nano- and microparticle powders in the spectral range of 320 to 1000 nm are presented in Fig. 2. TiO_2 powder has a sharp absorption peak in the near UV spectral region and lacks any absorption in the visible and NIR spectral regions. Al_2O_3 has constant ($\sim 20\%$) absorption in the visible and NIR regions that increases slightly in the near UV.

Figure 3 shows reflectance spectra of skin *ex vivo*. The solid curve corresponds to the reflectance spectrum of the intact skin. The absorption bands of blood hemoglobin at the wavelengths 416 nm (Soret band), 543 nm, and 578 nm⁴⁰ are very pronounced. The superposition of absorption and scattering properties of the used particles with that of skin forms the reflectance spectra of skin doped with the particles. The dashed curve represents the spectrum of the skin site after the FLMA and administering the suspension of TiO_2 nanoparticles. The depth of channels exceeded 300 μm ; therefore, the suspension from the channels was not removed totally. The change in the skin

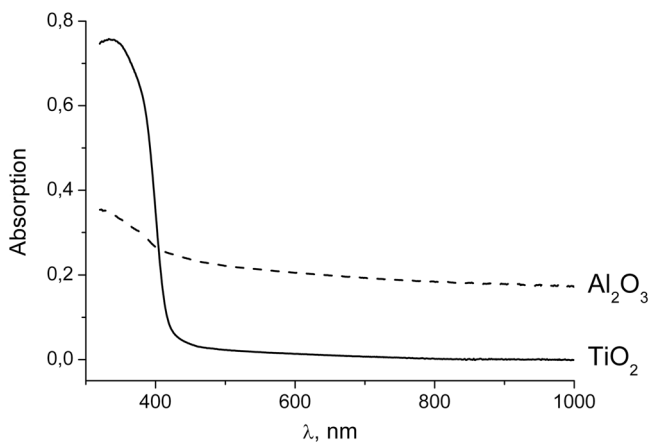


Fig. 2 Absorption spectra of the TiO_2 and Al_2O_3 powders.

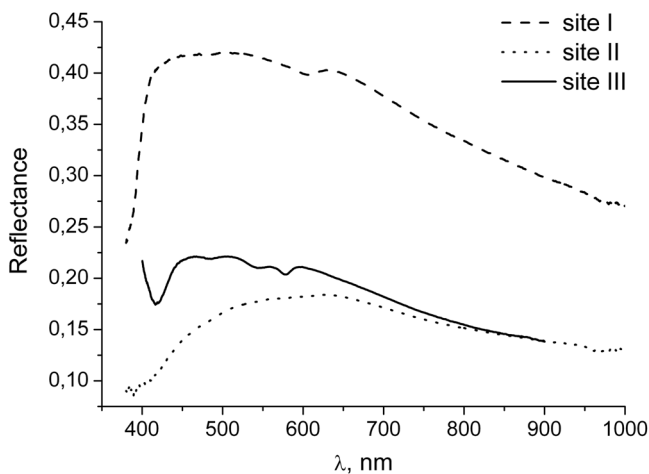


Fig. 3 Reflectance spectra of the *ex vivo* skin sample 2 h after FLMA and administering the TiO_2 suspension (the site I) and Al_2O_3 suspension (the site II) into skin, and intact human skin (the site III).

spectrum shape indicates the presence of some amount of TiO_2 nanoparticle suspension in the channels: the absorption band of TiO_2 in the near UV spectral region (see Fig. 2) induced significant decrease of the skin reflectance in this spectral range. The increase in the intensity of radiation reflected from the skin was observed, which is related to the substantial increase of the scattering coefficient of the tissue, promoted by the nanoparticles located in the microchannels. The dotted line corresponds to the reflectance spectrum of the skin site after FLMA and administering Al_2O_3 microparticle suspension. In this case, the decrease of the reflectance in near UV spectral region is also observed in correspondence with absorption band of Al_2O_3 micropowder (see Fig. 2).

3.3 In vivo Experiments

Figure 4 represents a series of photographs of the human skin sites treated with FLMA and particle suspensions. Image dimension is 12 \times 12 mm. The contrast of all images was increased by 50% for better visual perception of the treated sites. For that we

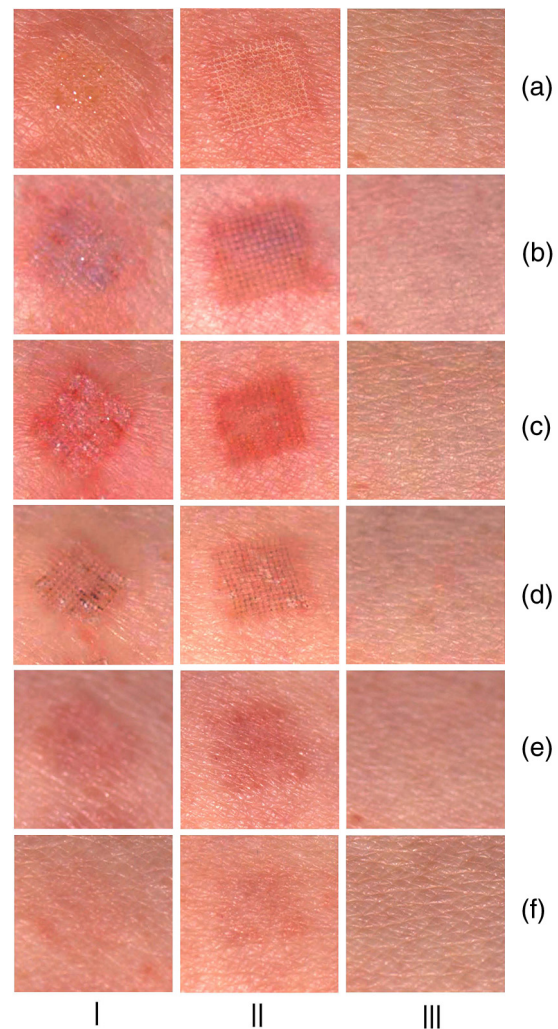


Fig. 4 Series of photographs of the human skin areas *in vivo*: site I was treated with FLMA and TiO_2 suspension; site II was treated with FLMA and Al_2O_3 suspension; and site III was treated with TiO_2 suspension. The images were obtained immediately after FLMA (a), 2 h (b); 24 h (c), 6 days (d), 14 days (e), and 30 days (f) after the treatments. Image size is 12 \times 12 mm.

used a formula⁴¹: $I_{out} = (I_{in} - dI) \cdot K + dI$, where I_{out} is the new value of intensity, I_{in} is the current value of intensity, dI is the average value of intensity in an image, and K is the contrast.

The first column of the images corresponds to the site treated with FLMA and TiO₂ suspension. The second one corresponds to the site treated with FLMA and Al₂O₃ suspension. The third one is the set of images of the site without FLMA. In this case, TiO₂ suspension was applied on the skin surface topically. This site was included in the study to model the use of TiO₂ as a component of sunscreens.

The images in the row (a) demonstrate the sites just after FLMA. The images Ia and IIa demonstrate well demarcated square treated areas resembling in appearance a lattice. Both erythema and slight edema in the areas of laser treatment were observed. In the image Ia, small lymph excretion took place. Blood excretion was not observed at either site.

In 2 h after the suspension application, the lightening of the skin was observed (see images Ib–IIIb). It was caused by the increase of skin reflection due to the particle suspension covering the surface. We also could see erythema and edema decreasing (see images Ib and IIb).

Twenty four hours later after the treatment, the complete healing of microchannels occurred. Treated sites were covered by a scab containing the particles. The openings of the channels filled up by the particles can be clearly seen (see images Ic and IIc). Some quantity of TiO₂ nanoparticles could have stayed in the sulci of skin (image IIIc).

In 6 days after the treatment, peeling of the damaged surface layer of epidermis and the restoration of the epidermis integrity was observed (see images Id and IIId). The scab on the skin surface remained. After 2 weeks, the microscopic channels were practically invisible; however, in the places of their location, slight redness was observed (see images Ie and IIe). In a month after the treatment, the pigmentation change was practically imperceptible (see images If and IIIIf). At this time point, no changes could be seen in the third site in comparison to baseline (images IIIId–IIIIf). It can be speculated that a total removing of the particles from the skin surface has occurred.

Figure 5 shows OCT images of the areas presented in Fig. 4. The depth and length of the scans correspond to 0.65 and 3 mm, respectively. In the images Ia and IIa, the sections of the ablated areas with microchannels are seen. The channels are marked with arrows. The image IIIa shows the OCT scan of the intact skin region. It is clearly seen that the skin microablation does not affect the optical depth of probing, which on average amounted to $\sim 320 \mu\text{m}$, close to the value of this parameter for intact skin. In the image for intact skin, a papillary structure of epidermis on the surface of the skin and a boundary between epidermis and dermis are clearly seen.

In the images Ib and IIb, the arrows indicate that ablation channels are filled up with the particle suspensions at the 2 h timepoint. The apparent depth of the microchannel filled with the particles (it is marked in the image Ib with an arrow) can be evaluated as 300 to 310 μm . Since the average refractive index of dermis is 1.37,⁴² the actual geometrical depth of the channel is

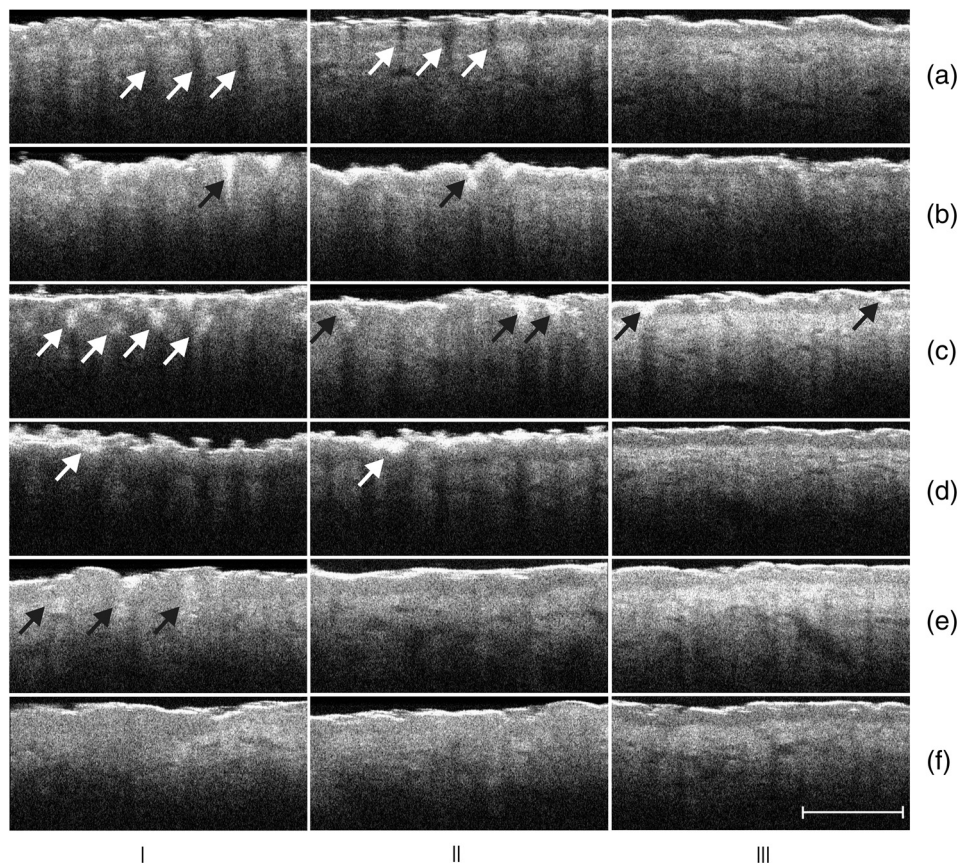


Fig. 5 Series of optical coherence tomography (OCT) images of the human skin areas *in vivo*: site I was treated with FLMA and TiO₂ suspension; site II was treated with FLMA and Al₂O₃ suspension; and site III was treated with TiO₂ suspension. The images were obtained immediately after FLMA (a), 2 h (b); 24 h (c), 6 days (d), 14 days (e), and 30 days after the treatments. Bar corresponds to 1 mm.

about 230 μm . The difference between channel depths *ex vivo* and *in vivo* can be explained by the following: the depth of penetration of nanoparticles can be noncoincident with that of the microscopic channels due to the healing of the channel walls in vital tissue. The image IIIb presents the skin covered with TiO_2 suspension. The application of nanoparticle suspension induced some reduction of the optical probing depth (on average, up to 180 μm). The reduction of the optical probing depth may be explained by the shielding effect produced by particle layer, located in the channels, on the skin surface, and in the skin appendage openings. This effect was due to their high reflectivity. As a result, the OCT signal from the dermis tissue decreased significantly.

The next row of images was obtained 24 h after the removal of the suspension from the skin surface. It has become evident that the microchannels are filled up with the suspension in depth (see images Ic and IIc). In the image IIIc, we can also see natural sulci of skin filled up with TiO_2 suspension. The localization of the particles is marked with arrows.

In the images Id and IId, which correspond to 6 days post-treatment, we can see the complete healing of microchannels. The peeling of the damaged surface layer of epidermis also begins at this point. On the skin surface, a scab containing particles (marked with arrows) forms a solid layer, which simulates a reflecting screen. Therefore, the optical probing depth decreases up to about 90 μm in the area of the microchannels and about 180 μm between them (see image Id) in the case of using the TiO_2 suspension. When the Al_2O_3 suspension was applied (see image IId), the optical probing depth in the area of the microchannels was $\sim 100 \mu\text{m}$, but in the area between them, the optical probing depth was equal with that of intact skin (see image IIIId). It is possible that large Al_2O_3 particles were removed from the skin surface almost completely and remained only in the channels, whereas the TiO_2 nanoparticles covered full treated surface.

Two weeks after the experiment, the peeling was completed (see images Ie and IIe). It can be suggested that bright sites in the OCT image Ie (marked with arrows) correspond to the closed microchannels still containing a quantity of nanoparticles. The image of intact skin (image IIIe) is identical to the initial one.

After the full restoration of the skin integrity (in a month), the particles, administered at the depth exceeding the epidermis thickness (100 to 150 μm), could stay in the dermis²⁵; however, their quantity was so little that they did not register in the OCT images. The optical probing depth for the images If, IIf, and IIIf was identical and coincided with that found before the experiment. However, sharp boundary between epidermis and dermis is absent in the images If and IIf unlike that in the image IIIf. In addition, blood vessels in the probing section of the skin are less visible. We hypothesize that the loss of the visualization contrast of epidermis and blood vessels in the OCT images can be related to the uniform distribution of the particles in the skin bulk.

Spectral measurements of skin (see Fig. 6) show differences in the reflectance of the studied skin sites related to the differences in fractions of light absorbed by the substances (see Fig. 2). We have chosen 24-h and 1-month time points for demonstration of changes in the reflectance skin spectra. Immediately after the laser treatment, both erythema and edema of the treated skin sites overshadowed the particle impact on the spectrum. In addition, the number of the particles on the skin surface was still too high to see the effects from in-depth

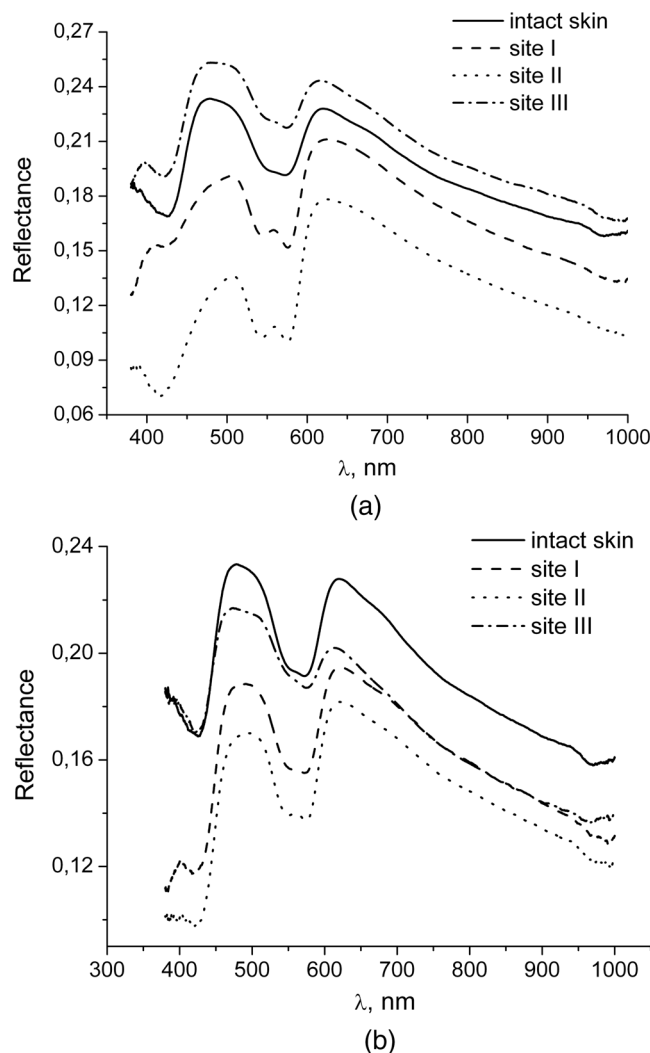


Fig. 6 Reflectance spectra of skin *in vivo* before (intact skin), 24 h post-treatment (a), and 30 days post-treatment (b) with laser microablation and administering the TiO_2 suspension (site I), Al_2O_3 suspension (site II), and administering TiO_2 suspension into intact skin (site III).

inserted nanoparticles. Later on, erythema and edema decreased gradually on the both skin sites, but also the amount of the particles decreased due to the peeling of the upper epidermal layer. In a month, only particles remaining in deeper skin layers induced the changes in the spectra.

Figure 6(a) demonstrates the reflectance spectra of skin *in vivo* before and 24 h post-treatment. Figure 6(b) shows reflectance spectra of the same skin sites 1 month after the treatment. The solid curve corresponds to the spectrum of intact skin before any treatment. We can see characteristic bands of blood absorption and a band of water absorption.⁴⁰ Some shift of the maxima of the blood peaks in skin spectrum *in vivo* in comparison with that *ex vivo* (see Fig. 3) is caused by different content of oxy- and deoxyhemoglobin in blood at *ex vivo* and *in vivo* measurements. Dashed curves are the spectra of skin from the site I after the FLMA and administering the suspension of TiO_2 nanoparticles. Dotted curves correspond to the spectra of skin from the site II after the FLMA and administering the suspension of Al_2O_3 microparticles. Dash-dot curves show the spectra of skin from the site III after an application of the suspension of TiO_2 nanoparticles on skin surface.

In 24 h, we can see the changes of skin spectrum relatively to that of intact skin caused by both the microablation of epidermal layer and particle presence [see Fig. 6(a), sites I and II]. Erythema of the studied site (see Fig. 4, row c) is seen as spectral shift and magnitude increase of the band related to oxyhemoglobin absorption (417, 542, and 574 nm). Besides, on the treated site, residual edema was observed that is seen as decreasing reflectance intensity in the range of water absorption. TiO₂ nanoparticles' presence is revealed as the appearance of the signal decreasing in the spectral range shorter than 400 nm. Dotted curve corresponding to the spectrum of skin on the site II demonstrates additional lowering of signal in comparison with that on the site I. It can be related to absorption of Al₂O₃ suspension in the visible spectral range (see Fig. 2). Dash-dot curve shows the spectrum of skin from the site III. At this site, skin was not damaged; therefore, the shape of the reflectance spectrum in visible and NIR spectral ranges coincides with that of intact skin. TiO₂ nanoparticles' presence is revealed as the decreasing reflectance in the short-wavelength range as well as general increasing of the reflectance for other wavelengths due to increase of scattering from the skin surface.

At 1-month time point, decreasing of reflectance from the both sites I and II in comparison with that of intact skin suggests the presence of residual erythema [see Fig. 6(b)]. From the shape of the spectra in the range shorter than 400 nm, it is well seen that the particles are totally absent on the skin surface (dash-dot curve) and present in deeper skin layers (dashed and dotted curves). The spectral measurements correlate with OCT data on the in-depth localization of nanoparticles.

4 Discussion

It was shown that the laser irradiation has great advantages in enhancing transdermal drug delivery of not only small but also large and hydrophilic molecules as well as nanoparticle suspensions.^{19,20,25,43,44} The permeation-enhancing mechanisms should be due to the photomechanical action, which leads to the SC damage. The damage character depends on laser wavelength, provided power density, pulse duration, exposure, etc.⁴³ We have used the device built on the basis of Er:YAG laser that emits light at 2.94 μm. This light is strongly absorbed by water molecules⁴⁰ that lead to skin microporation¹⁹ or fractional ablation²³ due to water explosive evaporation.

Ablative and nonablative fractional devices have been successfully employed for both skin rejuvenation and resurfacing in the field of laser treatment.^{23,45} Thermally induced microchannels of damage in the skin facilitate the formation of new collagen, elastin, hyaluronic acid, and other structural components.^{23,24,45} Depending on parameters of the radiation, the damage within these microchannels may consist of protein denaturation (e.g., of cellular metabolic enzymes or collagen) and/or ablation.²³

The microscopic examination of histological preparations allowed us to evaluate both depth and diameter of created microchannels and thickness of coagulated layer around a channel. A typical laser pulse resulted in channel formation with depth of about 300 μm and diameter of 50 to 70 μm. The thickness of coagulated collagen layer around a channel was in the range of 15 to 25 μm. This layer can prevent from quick release of the particle from the channel into surrounding tissue, thus the depot of the particles inside skin is created.

The laser microablation or any treatment related to skin damage induces local erythema, edema, and scabbing reactions of

skin. This effect is attributed to induced skin damage and aimed at reintegration of skin. Unfortunately, there are only a few articles that analyze these adverse effects. In Ref. 18, such adverse skin reactions as erythema and scabbing were observed in the local areas of skin affected by a sandpaper and immersion agents. Authors have evaluated the degree of erythema in 70 h after gentle rubbing with fine grit sandpaper and topical application of dextrose and glycerol as 23.6% and 11.7%, respectively, with respect to the total skin area previously optically cleared with dextrose and glycerol.

Based on digital images shown in Fig. 4, we have evaluated the dynamics of visible skin erythema in the sites I and II with respect to the erythema in the site III. To evaluate the relative erythema index (REI) on the studied areas, we used the following expression: $REI = \frac{1}{2} \left(\frac{R_z}{R_r} + \frac{B_z}{B_r} \right) - \frac{G_z}{G_r}$, where R_r , G_r , B_r are the area average values of the color coordinates in the control site (site II), and R_z , G_z , B_z are the area average values of the color coordinates in the sites treated with FLMA and particle suspensions (sites I and II). The color coordinates were obtained in the system RGB (red, green, and blue) with freeware IMAGEJ (National Institutes of Health, USA).⁴⁶ Results are shown in Table 1. Differences between REI of site I and site II are not significant. They can be referred to inaccuracy of measurements.

In Table 1, it is well seen that maximal value of REI was obtained at 24-h follow up. Evidently, this is related to formation of a scab on the damaged sites. Increasing of the REI in 14 days after the treatment is related to the peeling of the scab and appearance of regenerated skin (see Fig. 4, Ie and IIe). In 30 days after the treatment, erythema on the both evaluated skin sites decreased by 70% and 55% with respect to the maximal value of REI on the site I and site II, respectively. However, it remained noticeable. To decrease this unwanted skin reaction, the energy of laser pulse has to be reduced. But in this case, the depth of microchannels will be diminished. The compromise between unwanted skin reaction and desirable microchannel depth depends on specific aims.

For comparison, REI of the skin site treated with FLMA only was evaluated immediately after, in 6 days, and in 14 days post-treatment. The values were the following: REI = 42 ± 23, 30 ± 20, and 33 ± 18, respectively. The results have shown

Table 1 *In vivo* skin condition after fractional laser microablation and particle administering. Relative erythema index (REI) of affected area (sites I and II) was evaluated in relation to skin surface area without microablation (site III).

Time points	REI (± standard deviation)	
	Site I	Site II
Before the treatment	4 ± 14	1 ± 12
Immediately after the ablation	43 ± 20	53 ± 23
2 h	68 ± 23	66 ± 21
24 h	111 ± 29	85 ± 27
6 days	44 ± 11	40 ± 13
14 days	58 ± 23	61 ± 24
30 days	34 ± 13	38 ± 15

that in 6 days and 14 days, the difference between REI of the site treated with FLMA only and average value of REI of sites I and II is about 25% and 45%, respectively. Erythema decreased more slowly on the sites with the particle administering. Apparently, it was caused by an organism reaction on foreign inclusions.

We speculate that the erythema was not related to the particle toxicity. It is known that tattoo color ink particles can remain in skin during many years without any noticeable toxic effects. Al_2O_3 and TiO_2 particles are widely used in many topical skin care products.^{9,30,33} Overall, the current weight of evidence suggests that nanomaterials such as TiO_2 nanoparticles currently used in cosmetic preparations or sunscreens do not represent any elevated risk to human skin or human health.²⁸

The effect of nanoparticles on the optical properties of skin was studied in several publications. However, topical application of particle suspension promotes the distribution of the particles in skin not deeper than $3\ \mu\text{m}$ ³⁶ i.e., in superficial (horny) layer of human skin. Thus, the content of particles in skin decreases dramatically at the natural renewal of epidermal cells. Our study has shown that the use of the FLMA for TiO_2 and Al_2O_3 particles delivery into dermis can promote particle depositing in skin for a period longer than 1 month. It is followed from the Fig. 6(b), where the changes of the shape of the spectra in the short wavelength range are well seen.

It was shown that the image contrast of tissue layers increases after both gold^{20,26,47} and TiO_2 nanoparticles²⁶ administering. In particular, in Ref. 20, the reduction of intensity of the OCT signal, caused by the suspension of nanoparticles, applied to the skin surface or delivered into the skin, induced the increased contrast of imaging of the epidermis and the structure inhomogeneities located under the skin surface. The observations of OCT images described in Ref. 20 were made immediately after the particle administering, when the particles were not yet distributed uniformly in the skin bulk. In Ref. 26, the OCT images were registered after topical application of gold and TiO_2 nanoparticles. The fact that the presence of small amount of the particles on the skin surface increases contrast of OCT images is confirmed by the image IIIc in Fig. 5. Indeed, visualization of epidermis–dermis boundary in this image is better than in the image of intact skin (see image IIIa in Fig. 5).

The authors of the article⁴⁷ used microneedle technique to create the channels. The diameter ($70\ \mu\text{m}$) and the depth ($300\ \mu\text{m}$) of the channels were close to the corresponding parameters of the channels created with FLMA technique. However, microneedle channels did not have coagulated walls. The enhanced signals from the SC persisted over the entire 40 days because the nanoparticles were removed from the lower tissue due to metabolism and localized only in the SC. In the case of FLMA technique, the walls of the microchannels had coagulated layer²³ that prevented immediate diffusion of the particles outside the channels. However, it appears that during the month after the experiment, the particles left the channels and gradually distributed in dermis. Thus, general increasing of scattering in the skin bulk took place. As a result, optical heterogeneities disappeared in the OCT images (see images If and IIf in Fig. 5).

The differences between OCT images of skin with administered TiO_2 or Al_2O_3 are insignificant despite the fact that the values of refractive index of the substances vary considerably. For Al_2O_3 and TiO_2 , average refractive indices in the studied

spectral range are 1.69 and 2.3, respectively.³⁵ These values exceed significantly the refractive index of skin: the refractive indices of epidermis and dermis are 1.42 and 1.37, respectively.⁴² Therefore, in the OCT scans, the microchannels filled up by suspensions of the both particles look more or less equal.

5 Conclusion

This study shows that the use of FLMA with Er:YAG laser allows for efficient administering of TiO_2 nanoparticles ($<100\ \text{nm}$) and Al_2O_3 microparticles ($\sim 27\ \mu\text{m}$) into the dermis. At the pulse energy 3 J, the microscopic channels, created in the tissue by ablation, allowed for particle penetration up to $230\ \mu\text{m}$ deep into the dermis. The deep administration of the particles allows them to stay in the dermis for a prolonged period of time (longer than 1 month).

Based on digital photographs of the treated skin sites, we have evaluated the dynamics of visible skin erythema of the ablated skin sites with administered particles. It was shown that maximal value of the REI was obtained at 24-h follow up. In a month, erythema decreased significantly. On the both evaluated skin sites, it decreased by 70% (TiO_2 administering) and 55% (Al_2O_3 administering) with respect to the maximal value of the REI. Apparently, erythema was caused by an organism reaction on foreign inclusions.

The presence of the particles in the dermis affects the optical properties of the skin. During the month after the experiment, the particles left the channels and gradually distributed in dermis. Thus, the overall increase of scattering in the skin bulk took place. This technology can be used for controlling of skin appearance and for other medical and cosmetic applications.

Acknowledgments

The work was carried out under the partial support from the Russian Foundation for Basic Research (Grant Nos. 11-02-00560 and 12-02-92610-KO); Governmental contracts 14.B37.21.0563, 14.B37.21.0728, and 14.512.11.0022; project No. 1.4.09; FiDiPro, TEKES Program (40111/11), Finland; RF President's grant 1177.2012.2 "Scientific Schools." The authors wish to thank Palomar Medical Technologies Inc. for the grant of equipment, Dr. Vladislav V. Lychagov (Saratov State University, Russia) for his help in the measurements of the OCT images, and Dr. Alexey P. Popov (Oulu University, Finland) for his help in the measurements of the refractive indices of PEG-300.

References

1. G. Ceve and U. Vierl, "Nanotechnology and the transdermal route. A state of the art review and critical appraisal," *J. Contr. Release* **141**(3), 277–299 (2010).
2. J. Lademann et al., "Nanoparticles—an efficient carrier for drug delivery into the hair follicles," *Eur. J. Pharm. Biopharm.* **66**(2), 159–164 (2007).
3. S. Khandavilli and R. Panchagnula, "Nanoemulsions as versatile formulations for paclitaxel delivery: peroral and dermal delivery studies in rats," *J. Invest. Dermatol.* **127**(1), 154–162 (2007).
4. H. Schaefer and T. E. Redelmeier, *Skin Barrier*, Karger, Basel (1996).
5. R. Toll et al., "Penetration profile of microspheres in follicular targeting of terminal hair follicles," *J. Invest. Dermatol.* **123**(1), 168–176 (2004).
6. J. Lademann et al., "Determination of the cuticula thickness of human and porcine hairs and their potential influence on the penetration of nanoparticles into the hair follicles," *J. Biomed. Opt.* **14**(2), 021014 (2009).
7. A.C. Lauer et al., "Targeted delivery to the pilosebaceous unit via liposomes," *Adv. Drug Delivery Rev.* **18**(3), 311–324 (1996).

8. B. Baroli et al., "Penetration of metallic nanoparticles in human full-thickness skin," *J. Invest. Dermatol.* **127**(7), 1701–1712 (2007).
9. J. Lademann et al., "Penetration of titanium dioxide microparticles in a sunscreen formulation into the horny layer and the follicular orifice," *Skin Pharmacol. Appl. Skin Phys.* **12**(5), 247–256 (1999).
10. A. Rolland et al., "Site-specific drug delivery to pilosebaceous structures using polymeric microspheres," *Pharm. Res.* **10**(12), 1738–1744 (1993).
11. A. K. A. Silva et al., "Magnetophoresis at the nanoscale: tracking the magnetic targeting efficiency of nanovectors," *Nanomedicine* **7**(11), 1713–1727 (2012).
12. S. E. Lee et al., "Penetration pathways induced by low-frequency sonophoresis with physical and chemical enhancers: iron oxide nanoparticles versus lanthanum nitrates," *J. Invest. Dermatol.* **130**(4), 1063–1072 (2010).
13. S. Lee et al., "Photomechanical delivery of 100-nm microspheres through the stratum corneum: implications for transdermal drug delivery," *Laser Surg. Med.* **31**(3), 207–210 (2002).
14. M. Kendall et al., "Effects of relative humidity and ambient temperature on the ballistic delivery of micro-particles to excised porcine skin," *J. Invest. Dermatol.* **122**(3), 739–746 (2004).
15. A. Tezel, A. Sens, and S. Mitragotri, "Incorporation of lipophilic pathways into the porous pathway model for describing skin permeabilization during low-frequency sonophoresis," *J. Contr. Release* **83**(1), 183–188 (2002).
16. A. R. Denet, R. Vanbever, and V. Preat, "Skin electroporation for transdermal and topical delivery," *Adv. Drug Deliv. Rev.* **56**(5), 659–674 (2004).
17. N. Roxhed et al., "Painless drug delivery through microneedle-based transdermal patches featuring active infusion," *IEEE Trans. Biomed. Eng.* **55**(3), 1063–1071 (2008).
18. O. Stumpp, B. Chen, and A.J. Welch, "Using sandpaper for noninvasive transepidermal optical skin clearing agent delivery," *J. Biomed. Opt.* **11**(4), 041118 (2006).
19. Y. G. Bachhav et al., "Effect of controlled laser microporation on drug transport kinetics into and across the skin," *J. Contr. Release* **146**(1), 31–36 (2010).
20. G. S. Terentyuk et al., "Use of fractional laser microablation and ultrasound to facilitate the delivery of gold nanoparticles into skin in vivo," *Quantum Electron.* **42**(6), 471–477 (2012).
21. O. Lademann et al., "Simulation of the penetration of particles into skin by plasma tissue interaction," *Laser Phys. Lett.* **8**(10), 758–764 (2011).
22. J. Enfield et al., "In vivo dynamic characterization of microneedle skin penetration using optical coherence tomography," *J. Biomed. Opt.* **15**(4), 046001 (2010).
23. B.D. Zelickson et al., "Semi-automated method of analysis of horizontal histological sections of skin for objective evaluation of fractional devices," *Lasers Surg. Med.* **41**(9), 634–642 (2009).
24. H.-J. Laubach et al., "Skin responses to fractional photothermolysis," *Lasers Surg. Med.* **38**(2), 142–149 (2006).
25. E. A. Genina et al., "Fractional laser microablation of skin aimed at enhancing its permeability for nanoparticles," *Quantum Electron.* **41**(5), 396–401 (2011).
26. M. Kirillin et al., "Contrasting properties of gold nanoshells and titanium dioxide nanoparticles for optical coherence tomography imaging of skin: Monte Carlo simulations and in vivo study," *J. Biomed. Opt.* **14**(2), 021017 (2009).
27. A. Lemelle et al., "Application of gold nanoparticles as contrast agents in confocal laser scanning microscopy," *Laser Phys. Lett.* **6**(1), 71–75 (2009).
28. A. V. Zvyagin et al., "Imaging of zinc oxide nanoparticle penetration in human skin in vitro and in vivo," *J. Biomed. Opt.* **13**(6), 064031 (2008).
29. A. P. Popov et al., "TiO₂ nanoparticles as an effective UV-B radiation skin-protective compound in sunscreens," *J. Phys. D Appl. Phys.* **38**(15), 2564–2570 (2005).
30. A. Weir et al., "Titanium dioxide nanoparticles in food and personal care products," *Environ. Sci. Technol.* **46**(4), 2242–2250 (2012).
31. J. Lademann et al., "Investigation of the stability of coated titanium microparticles used in sunscreens," *Skin Pharmacol. Appl. Skin Physiol.* **13**(5), 258–264 (2000).
32. M. Lualdi et al., "A phantom with tissue-like optical properties in the visible and near infrared for use in photomedicine," *Lasers Surg. Med.* **28**(3), 237–243 (2001).
33. L. C. Becker Cosmetic ingredient review, "Safety assessment of alumina and aluminum hydroxide as used in cosmetics," http://www.cir-safety.org/sites/default/files/Alumin_032013.pdf (11 February 2013).
34. "Applications and use of integrating spheres with the LAMBDA 650 and 850 UV/Vis and LAMBDA 950 UV/Vis/NIR spectrophotometers," Application Note UV/VIS and UV/VIS/NIR Spectroscopy, www.perkinelmer.com (25 May 2013).
35. I. K. Kikoin, *Tables of Physical Quantities*, I. K. Kikoin, Ed., Atomizdat, Moscow (1976).
36. A. P. Popov et al., "Effect of multiple scattering of light by titanium dioxide nanoparticles implanted into a superficial skin layer on radiation transmission in different wavelength ranges," *Quantum Electron.* **37**(1), 17–21 (2007).
37. Thorlabs, *Spectral Radar OCT Systems*, http://www.thorlabs.com/images/Catalog/V19_07_Micros_Img.pdf (21 January 2013).
38. A. Knüttel and M. Boehlau-Godau, "Spatially confined and temporally resolved refractive index and scattering evaluation in human skin performed with optical coherence tomography," *J. Biomed. Opt.* **5**(1), 83–92 (2000).
39. V. V. Tuchin, *Tissue Optics: Light Scattering Methods and Instruments for Medical Diagnostics*, SPIE Press, Bellingham (2007).
40. A. N. Bashkatov et al., "Optical properties of human skin, subcutaneous and mucous tissues in the wavelength range from 400 to 2000 nm," *J. Phys. D Appl. Phys.* **38**(15), 2543–2555 (2005).
41. G. Y. Shliht, *Digital Processing of Colour Images*, Addison-Wesley, Reading (1995).
42. H. Ding et al., "Refractive indices of human skin tissues at eight wavelengths and estimated dispersion relations between 300 and 1600 nm," *Phys. Med. Biol.* **51**(6), 1479–1489 (2006).
43. C. Liu et al., "1064 nm-Nd:YAG lasers with different output modes enhancing transdermal delivery: physical and physiological mechanisms," *J. Biomed. Opt.* **18**(6), 061228 (2013).
44. J.-Y. Fang et al., "Enhancement of topical 5-aminolaevulinic acid delivery by erbium:YAG laser and microdermabrasion: a comparison with iontophoresis and electroporation," *Br. J. Dermatol.* **151**(1), 132–140 (2004).
45. D. Manstein et al., "Fractional photothermolysis: a new concept for cutaneous remodeling using microscopic patterns of thermal injury," *Lasers Surg. Med.* **34**(5), 238–426 (2004).
46. W. Rasband "ImageJ," <http://imagej.nih.gov/ij> (25 June 2013).
47. C. S. Kim et al., "Enhanced detection of early-stage oral cancer in vivo by optical coherence tomography using multimodal delivery of gold nanoparticles," *J. Biomed. Opt.* **14**(3), 034008 (2009).